Earth Sciences
2021; 10(6): 275-280
http://www.sciencepublishinggroup.com/j/earth
doi: 10.11648/j.earth.20211006.13
ISSN: 2328-5974 (Print); ISSN: 2328-5982 (Online)

Statistical Regularity and Relation Between Small Earthquakes and Crustal Velocity Structure Beneath Bohai Sea and Its Surrounding Areas in China

Zhu Xinran, Xue Peng, Wang Wei, Ni Yingying, Pang Guanghua*

College of Electrical and Electronic Engineering, Changchun University of Technology, Changchun, China

Email address:
Zhu_xin_ran@163.com (Zhu Xinran), pghua7@163.com (Pang Guanghua)
*Corresponding author

To cite this article:
Zhu Xinran, Xue Peng, Wang Wei, Ni Yingying, Pang Guanghua. Statistical Regularity and Relation Between Small Earthquakes and Crustal Velocity Structure Beneath Bohai Sea and Its Surrounding Areas in China. *Earth Sciences*. Vol. 10, No. 6, 2021, pp. 275-280.
doi: 10.11648/j.earth.20211006.13

Received: October 4, 2021; **Accepted**: November 8, 2021; **Published**: November 12, 2021

Abstract: The Bohai Sea is a seismically active region in China, and the studying of the velocity structure of Bohai Sea and its relationship with earthquake may be helpful to the analysis and prediction of earthquakes. Now, ambient noise tomography is an effective tool to obtain crust and upmost mantle structure. In this paper, the S-wave velocity model of the crust beneath the Bohai Sea and its surrouding areas in China was constructed applying ambient noise tomography method, with steps of calculating cross correlations of all possible vertical-component data recorded in 2013 year, retrieving Empirical Green's Functions (EGFs) for Rayleigh wave, measuring and assessing phase velocity-dispersion curves, creating the phase-velocity maps for the 8-35 s period of the Rayleigh wave, constructing the phase velocity maps and inverting the S-wave velocity structure. We work on the statistics and analysis of the characteristic relationship between crustal S-wave velocity and the temporal and spatial distribution of small earthquakes. The results from all available vertical profiles along different directions reveal that small earthquakes usually occur at the edge of the low-velocity anomaly within the shallow crust in a certain velocity range and, under special conditions, even in a distinct velocity contour. The locations of occurrence are closely related to undulating changes of the corresponding Moho morphology and the locally high Vs anomalies within the middle crust.

Keywords: Crust Structure, Small Earthquakes, Regularity, Relation, Bohai Sea

1. Introduction

Bohai sea is the area of the most intensive seismic activity in the eastern continental margin and bay of the country, which is just the intersection of northeast Tanlu seismic belt and northwest Zhangjiakou Bohai seismic belt [1, 2]. There have been many strong earthquakes in history, with high intensity and frequency of seismicity. In particular, the incidence of major earthquakes above M ≥ 7 is the highest in North China seismic area, with an average of once in 120 years [3-5]. Such as the 7.4 magnitude earthquake of 1969 [6, 7]. An earthquake with a magnitude of 7.3 occurred in 1975 in near Chagou (40°42'N, 122°E), approximately 20 km southeast of the Haicheng [8]. Between 1999 and 2000, two earthquakes with magnitudes 5.1 and 5.4 occurred on the border between Haicheng and Xiuyan. On the contrary, the occurrence frequency of earthquake in Liaodong Bay in the north of Bohai Sea is small, especially moderately strong earthquakes.

At present, many research achievements have been made in the study of seismicity in the Bohai Sea, but most of these achievements are to explore the plane distribution characteristics of seismicity and its relationship with seismotectonics [3, 9-11]. What is more, previous studies have shown that the occurrence of earthquakes is closely related to the structure and properties of regional crust and upper mantle [12-18]. Consequently, it is of great significance to study the velocity structure of active seismic structural belt for detecting the law of seismic activity.

2. Data and Methods

The data, methods, time-domain analysis, checkerboard test, image technique and S-wave inversion in this paper are introduced in this part. The preprocessing scheme became mature [19, 20], and the data prcessing followed Bensen et al [21].

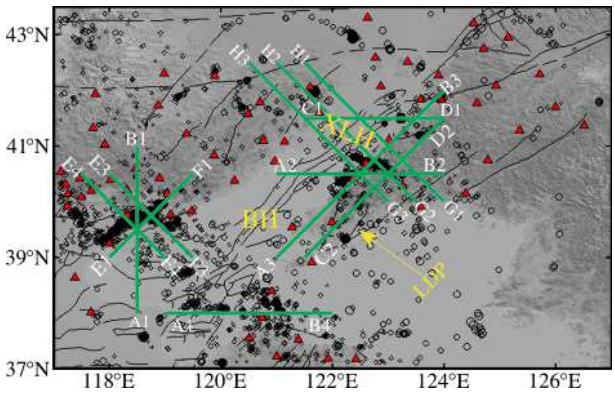

Figure 1. *The Spatial distribution of broadband seismic stations, the epicentre distribution of small earthquakes and background structure of the studied area. XLH represents Xialiaohe Basin. BH represents Bohai Sea. LDP represents Liaodong Peninsula. The red triangles represent broadband stations. Black hollow circles denote seismic events in 2008-2015. All events have ML<4.5 and a focal depth≦42 km. The size of the circle is proportional to the magnitude of the earthquake.*

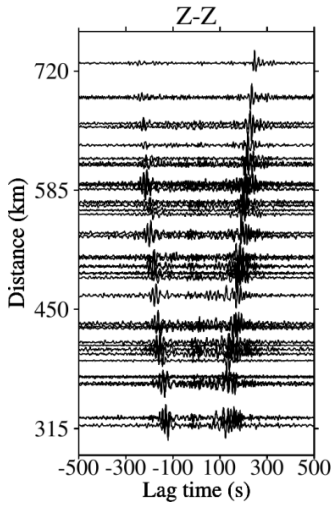

Figure 2. *3-40 s band-pass-filtered record between station LZH and other stations with vertical-vertical cross-correlations.*

The mean of the continuous vertical-component seismic waveform data was first removed, and the instrument response were removed from the daily noise time series. Next, all records were filtered in period band 2.25 and 60 s. Then, the time-domain normalization is carried out to suppress the influence of earthquake signals and other irregularities using a weighted running average method. Lastly, we performed the spectral whitening to avoid significant spectral imbalance and to broaden the flatted spectra over the entire period band. After the data was processed as daily records at each station using the above steps, we calculated cross-correlationds between all possible station pairs. Subsequently, the obtained daily cross-corrrelations were stacked to the final asymmetric cross-correlation results including positive branch and negative branch, and the positive and negative branches of the cross-correlations were stacked to form the symmetric cross-correlations and improve the signal-to-noise ratio (SNR). At last, a negative time derivative was accepted to gain the Empirical Green's Function (EGF) of the Rayleigh wave from Z-Z cross-correlations. Figure 2 presents Z-Z asymmetric cross-correlations between station LZH and other possible stations. The phase-velocity dispersion curves for Rayleigh wave were attained by applying the technique exploited by Yao et al [22], which can quickly follow up the entire dispersion curve. We showed examples of the four phase-velocity dispersion curves and their cross-correlations and ray distribution in Figure 3. Then We carried out quality control by filtering criteria for reliability of subsequent imaging. First, the dispersion measurements were discarded with SNR less than five at an individual period. The average SNRs of Z-Z cross-correlations are detected in Figure 4. The average SNRs decrease from the periods at 14 s. Second, the dispersion measurements with path lengths ≥3 wavelengths were only accepted to avoid spurious signals from interference between the causal and anticausal parts [23, 24]. Third, on the basis of the reasonable morphological character of the dispersion curves according to the cluster analysis [25], dispersion curves were visually inspected, and inconsistent ones or notable abnormal ones were discarded.

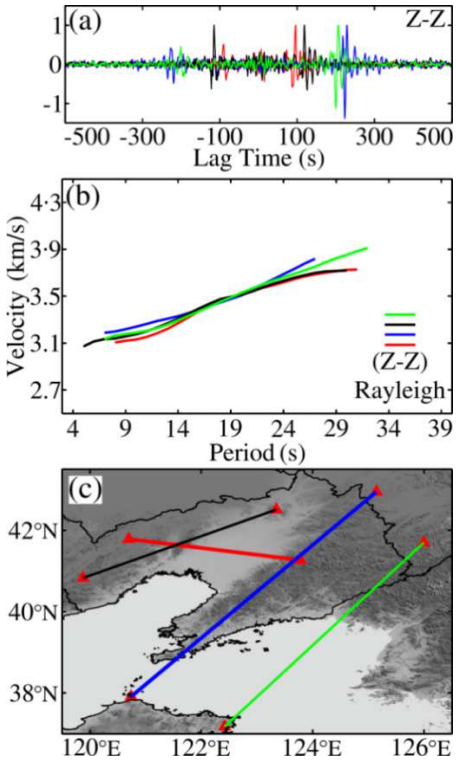

Figure 3. *Examples of the phase-velocity dispersion curves. (a) The 2.25-60 s band-pass-filtered cross-correlations for Z-Z. Z denotes vertical section. (b) Phase-velocity dispersion curves; the solid lines denote phase-velocity dispersion curves of the Rayleigh waves; (c) The interstation paths for the phase-velocity measurements. The coloured waveforms in (a), the coloured curves in (b) and the rays in (c) correspond to each other.*

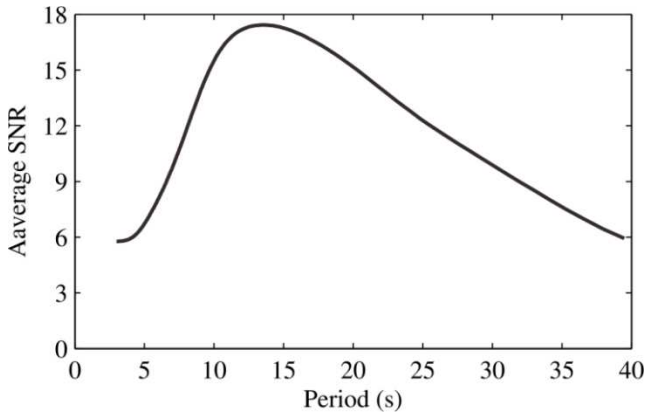

Figure 4. *The average SNRs of Rayleigh wave cross-correlations.*

Before Rayleigh-wave velocities invertion, the checkerboard tests were done to validate the dependability of the later imaging. The 1.5° × 1.5° cell was as the true theoretical velocity model, i.e. the alternating size of high-speed and low-speed unit was 1.5°. What is more, each unit was allocated 5% positive or negative speed disturbance, and the average speed in different periods was 4 km / s. Lastly, the synthetic data of velocities were computed based on the actual paths of station pairs at each period. The checkerboard tests in period band 3-40 s based on the true path coverage are established. Generally, checkerboard recovery is reasonably good for regions with dense rays. Nevertheless, smearing effects still exist at edges. In this study, the checkerboard-test results for the Rayleigh-wave phase velocity in period band 8 - 35 s display that the input model can be restored satisfactorily in most areas of the studied area. Lastly, the selected dispersions between 5 s and 35 s periods were used to invert for lateral 2-D velocity maps by the tomographic technique of Tarantola et al. [26] and Yao et al. [22, 27, 28].

The Rayleigh-wave dispersion curves at the divided node with the 0.5°×0.5° were extracted from the dispersion curves between the station pairs. Then the dispersion curve at each node from the previous step was inverted to the 1dimension (1 D) shear-wave (S-wave) velocity structure under corresponding node using the technology described in detail by Herrmann and Ammon [29] with linear steps. It is well known that surface-wave dispersion measurement is mostly sensitive to S-wave velocity. Therefore, in our inversion, only the S-wave velocity of each layer is taken as the inversion parameter, the P-wave velocity and density are derived from the empirical formulas. Layered Earth models from the depth to 46 km with respect to the halfplace model were employed, and the Moho depth parameter was referring to the recent receiver function works [30, 31]. The inversion program was repeated five times, and most grid units can match the Rayleigh-wave dispersion curves very well. That is, the fifth inversion results were taken as the final 1D S-wave profile. Finally, the collection of all inverted 1D profiles was compiled to 3D S-wave velocity structures.

3. Results and Discussion

3.1. Vertical Profiles of S-wave Velocity - 1

The vertical interface morphology of velocity structure in the south of Liaoning Province are displayed in Figure 5. There is an obvious correlation between the observed velocity structure and the known geological characteristics. More specifically, the low-velocity anomaly near the surface reflects the deposition and subsidence of the Xialiaohe Basin in Mesozoic and Cenozoic; the high velocity anomaly suggests the mantle uplift of the Xialiaohe Basin, furthermore, the H2-G2 and H3-G3 profiles display upper mantle upwelling with gentle slope in northwest and steep slope in southeast.

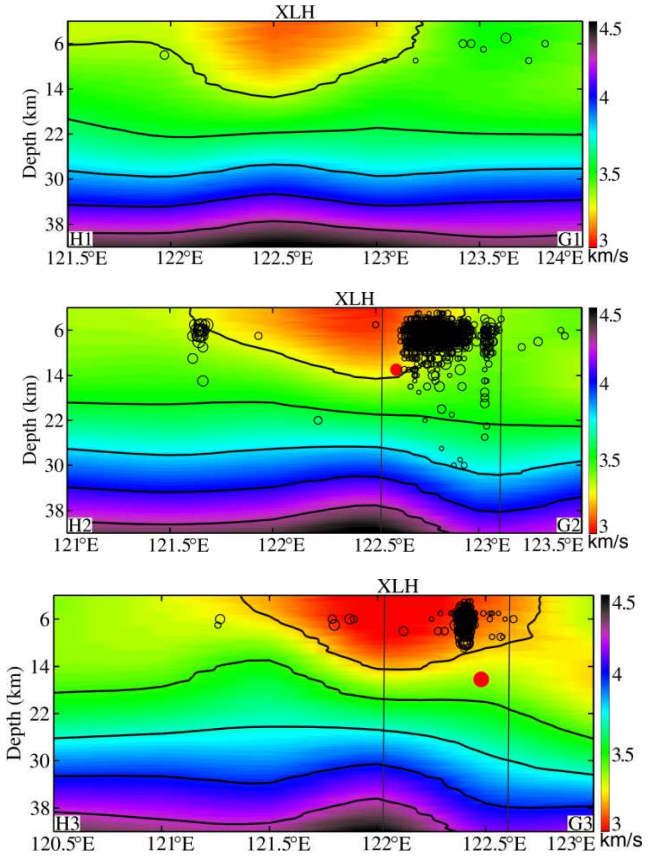

Figure 5. *S-wave velocity structures along the profiles of H1-G1, H2-G2 and H3-G3 (positions of the profiles as demonstrated in figure 1). Black hollow circles indicate seismic events in 2008-2015 years; (H2-G2) Solid red circle indicates the Haicheng earthquake with Ms 6.0 in 1978; (H3-G3) Solid red circle indicates the Haicheng earthquake with Ms 7.5 in 1978; all events with ml>2 and distance less than 0.1768° from the profile are on the same profile. XLH: Xialiaohe basin; black lines represent velocity isolines.*

Another apparent feature revealed by the profiles H2-G2 and H3-G3 is that the majority of small earthquakes occurred in the low-velocity anomaly region, which coincides with the southeastern slope of the mantle uplift — the faster uplift (between the two vertical lines in profiles H2-G2 and H3-G3). Therefore, this may be caused by the difference of crustal tectonic activities under the unified regional tectonic stress field, meanwhile, the relatively broken unit (the low-velocity anomaly) in the

upper crust offers favorable factor. Furthermore, the small earthquakes in the eastern margin of Xialiaohe Basin are frequent and relatively diffused (black circle in profile H2-G2). This may be due to some of the fact that the low velocity weak zone creates conditions for stress concentration in the surrounding rigid medium to brittle fracture or stick-slip. On the contrast, there is no corresponding relationship in profile H3-G3 affected by influence of the high-speed middle crust, obstructing of material convection. What is more, there is another phenomenon that the Haicheng earthquake with a magnitude of 7.3 in 1975 and the Haicheng earthquake with a magnitude of 6.0 in 1960 (the black solid circles in profiles H2-G2 and H3-G3, respectively) also occured in these slopes. To summarize, the shallow earthquakes occurred in the shallow crustal low-velocity zone, and there is a correspondence with the southeast slope of the upper mantle uplift belt.

The left side and right side of the XLH basin are West Liaoning and East Liaodong, respectively. From the contour lines in profiles H2-G2 and H3-G3, we can see that the velocity from the middle and lower crust and Moho nearby in the West Liaoning is slower than those in East Liaoning. That is to say, there are obvious differences in the development characteristics of the two wings of Liaodong and Western Liaoning. The characteristics of velocity structure in southern Liaoning are basically consistent with the results of Luyang-Haicheng-Donggou section [32].

3.2. Vertical Profiles of S-wave Velocity - 2

Different types of distribution characteristics of small earthquakes have significant differences as follows: (i) Figures. 6a1-2a4: The two dotted lines in Figs. 6 a1, a3 and a4 showthat the distribution of small earthquakes coincides with the peak of the top layer of localized high Vs anomalies within the middle crust. Relatively local and high Vs anomalies, almost belonging to brittle medium, are favourable for the concentration of stress in the upper crust, which may partly be the cause for occurrence of earthquake swarms. However, there exists a notable shift of small earthquakes to the left of the two dashed lines in Figure 6 a2, which may reflect an effect of the somewhat higher velocities (HV) on the right side of the earthquakes. More specifically, the high velocities (HV) signify large rigidity and hinder material convection. (ii) Figs. 7 b1 and b2: The distinctive feature is that the small earthquakes occur in certain velocity contours, and even repeatedly occur (profile C1-D1 in Figure 7b1). In addition, the Moho below the small earthquakes has relatively small lateral undulations. (iii) Figures. 8 c1-c4: The velocity contours clearly indicate that the small earthquakes cluster in the velocity range from 3.23 to 3.32 km/h. Moreover, the corresponding thickness of the crust changes rapidly. On the whole, seismic activity is strong link to change of crustal thickness and high Vs anomalies within middle crust.

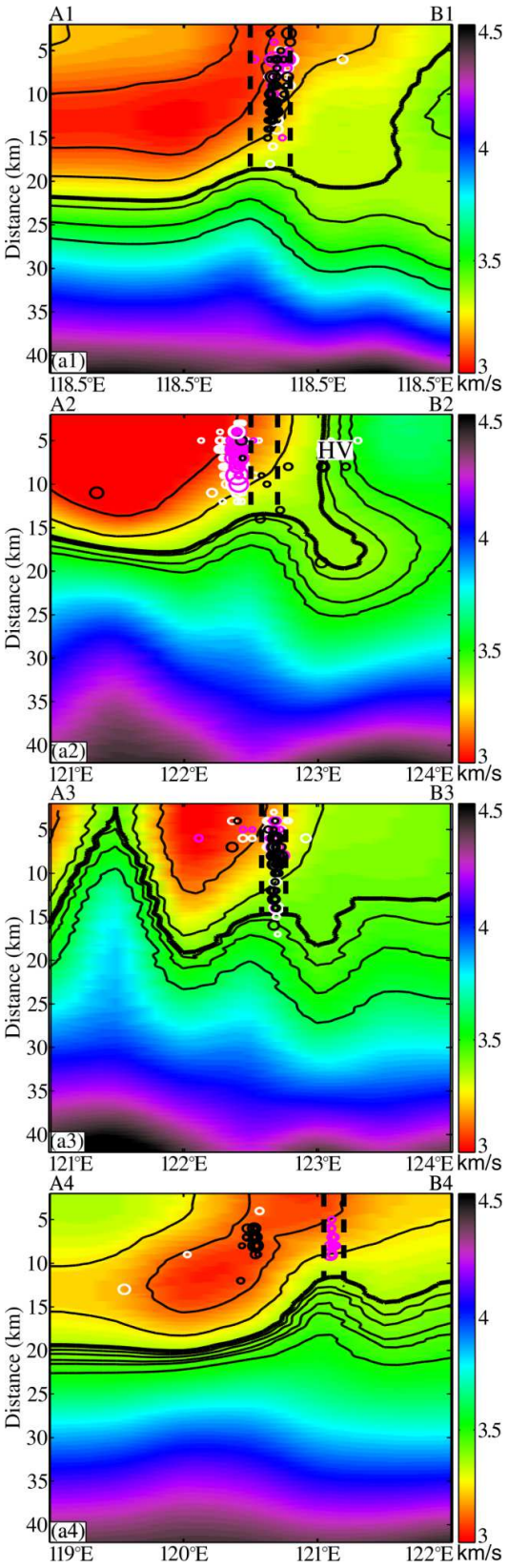

Figure 6. *S-wave velocity images along the profiles A1B1, A2B2, A3B3, and A4B4. (positions of the profiles as demonstrated in Figue 1). Black hollow circles, blue hollow circles and white hollow circles indicate seismic events in years 2008-2010, 2011-2012 and 2013-2015, respectively; all events with ML<4.5 and distances less than 0.01° from the profile are on the same profile. Figure 2a2, HV: high velocity. Black lines represent velocity isolines.*

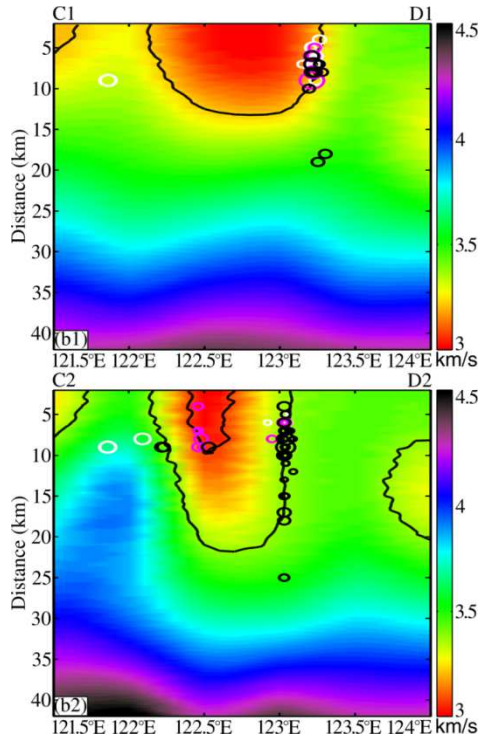

Figure 7. *S-wave velocity images along the profiles C1D1 and C2D2. (positions of the profiles as demonstrated in Figure 1). Black hollow circles, blue hollow circles and white hollow circles indicate seismic events in years 2008-2010, 2011-2012 and 2013-2015, respectively; all events with ML<4.5 and distances less than 0.01° from the profile are on the same profile.*

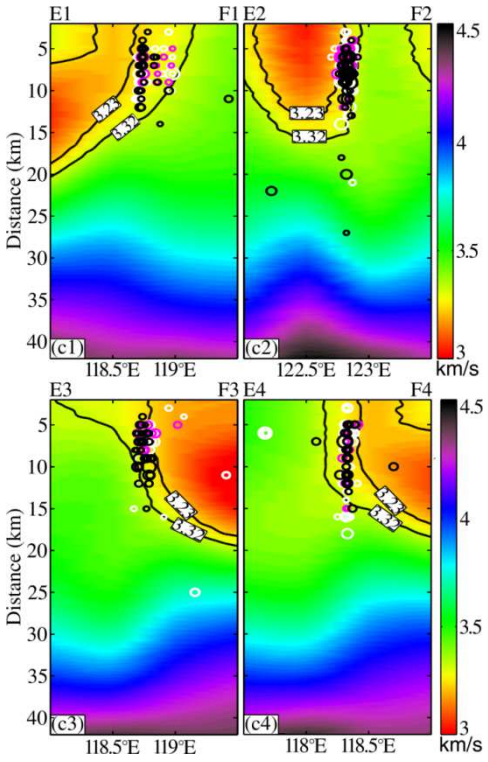

Figure 8. *S-wave velocity images along the profiles E1F1, E2F2, E3F3, and E4F4. (positions of the profiles as demonstrated in Figure 1). Black hollow circles, blue hollow circles and white hollow circles indicate seismic events in years 2008-2010, 2011-2012 and 2013-2015, respectively; all events with ML<4.5 and distances less than 0.01° from the profile are on the same profile.*

Figures 6-8 shows that the distribution characteristics of small earthquakes have certain commonalities: (i) small earthquakes mainly occur in shallow crust, and they are centralized with vertical linearity in the space, indicating that deeper and shallower motions are linked, perhaps with one set triggering the other. (ii) Small earthquakes cluster at the the low-velocity edge zone of the basement velocity structure, most velocity structures of bottom crust and the Moho morphology that small earthquakes correspond to show undulating changes obviously. This paper only explores the relationship between small earthquakes and the velocity structure in the local area. Expansion of the study area of earthquake-prone regions, in combination with prior results and more geological and geophysical data, to jointly analyse and explain the overall results will be a natural extension of this study.

4. Conclusions

In this paper, we conducted the Rayleigh wave phase-velocity maps of China's Bohai Sea and its adjacent areas using ambient noise. The S-wave velocity structure was inverted from Rayleigh wave dispersion maps extending to a depth of 42 km. The S-wave velocity maps show particularly strong heterogeneity and are in excellent agreement with known geological surface features. Moreover, based on analyzing the relationship between crustal structure and distribution of small earthquakes, we find that the seismic activity is closely related to the intracrustal velocity structure. The main observable phenomena are as follows:

(1) The earthquake swarms in Xialiaohe Basin tend to concentrate in the low-velocity boundaries, locating on the northwest-wing slope (steeper slope) of the upper mantle uplift belt. The low-velocity zone, signifying weak and soft stratum, paves the way for the brittle rock fracturing or stick-slip taking place.

(2) The distribution of a few small earthquakes correlates with the top of the upper layer of localized high Vs anomalies within the middle crust, probably resulting from the high Vs anomalies facilitating the accumulation of stress at the top of the upper crust.

(3) Some earthquakes occur in certain velocity contours, and the lower part of the crust just below the earthquakes has small undulating changes. And some occur in distinct velocity ranges above the deep slope belt of crustal thickness.

Acknowledgements

We express sincere thanks to the State Earthquake Information Service-Data Management Center for providing the data. We appreciate Dr. Huajian Yao for providing the related codes. This research is supported by 2021 innovation and entrepreneurship training program of college students in Changchun University of Technology (project number: 2021cxcy053).

References

[1] Qi J F, Deng R J, et al. 2008. Structural characteristics of the Tan-Lu fault zone in Cenozoic basins offshore the Bohai Sea. Science in China Series D: Earth Sciences.

[2] Qi J F, Yang Q. 2010. Cenozoic structural deformation and dynamic processes of the Bohai Bay basin province, China. Marine and Petroleum Geology. 27: 757-771.

[3] Huan W L, Wang S Y, Chang X D, et al. 1989. Characteristics of seismicity of Bohai Sea. Journal of Seismological Research (in Chinese). Vol. 12. No. 1. 1-9.

[4] Lv Y J, Tang R Y, Peng Y J, Xu G L. 2003a. Study on engineering earthquake of Bohai Oilfield. Beijing: Seismological publishing house.

[5] Lv Y J, Peng Y J, Sha H J. 2003b. Seismicity Environment in Bohai and its Adjacent Regions. Bulletin of the Institute of Crustal Dynamics. (in Chinese). Issue 1 (7): 38-44.

[6] Xu J, Gao Z W, Sun J B, et al. 2001. Analysis of structures in 1969 Bohai Sea Ms 7.4 earthquake area and discussion about the causative structure (in Chinese). Earthq Res China, 17: 121–133.

[7] Fu Z, Liu J, Liu G. 2004. On the long-term seismic hazard analysis in the Zhangjiakou-Penglai seismotectonic zone, China. Tectonophysics, 390: 75–83.

[8] Zhu F M. 1980. The Haicheng Earthquake in 1975. Seismological Press, Beijing. 165-195 (in Chinese).

[9] Wei G X, Ji T R. 1990. A review of the researches in the Bohai Sea Earthquake. Journal of Disaster Prevention and Mitigation Engineering. (in Chinese). (03): 1-5.

[10] Wei G X, et al., 1993. Study on seismicity of Tan Lu belt. Beijing: Seismological publishing house. (in Chinese)

[11] Wang H L, Wang Y G, Liu X Q, et al., Study on fault tectonics and strong seismicity in Bohai and its adjacent regions. Journal of seismological research. (in Chinese). 23 (1); 35-43.

[12] Yu X W, Chen Y T, Zhang H. 2010. Three-dimensional crustal P-wave velocity structure and seismicity analysis in Beijing-Tianjin-Tangshan region. Chinese J. Geophys. (in Chinese). 53 (8): 1817-1828. Doi: 10.3969/j.issn.0001-5733. 2010.08.007.

[13] Wang C Z, Wu J P, Fang L H, et al. 2013. The relationship between wave velocity structure around Yushu earthquake source region and the distribution of aftershocks. Chinese J. Geophys. (in Chinese). 56 (12): 4072-4083. doi: 10.6038/ cjg 20131212.

[14] Obermann, B. Froment, M. Camillo, et al. 2014. Seismic noise correlations to image structural and mechanical changes associated with the Ms 7.9 2008 Wenchuan earthquake. Journal of Geophysical Rese arch.

[15] Jiang D D, Jiang W W, Xu Y, et al. 2014. Characteristics of crustal structure and their relation with major earthquakes in western China. Chinese J. Geophys. (in Chinese). 57 (12): 4029-4040, doi: 10.60 38/cjg20141215.

[16] Xu T, Zhang M H, Tian X B, et al. 2014. Upper crustal velocity of Lijiang-Qingzhen profile and its relationship with the seismogenic environment of the Ms 6.5 Ludian earthquake. Chinese J. Geophys. (in Chinese), 57 (9): 3069-3079, doi: 10.6038/cjg20140932.

[17] Yu N, Wang X B, Hu X Y, et al. 2014. The deep geophysical structure of the middle section of the Longmen mountains tectonic belt and its relationship to the Wenchuan earthquake. Acta geologica sinica (English Edition).

[18] Zhang J S, Wang F Y, Liu B F, et al. 2014. A study of the crustal-mantle velocity structure beneath the Yushu earthquake zone and its adjacent areas. Seismology and geology. (in Chinese). Vol. 36, No. 2 doi: 10.3969/j.issn.0253-4967.2014.02.004.

[19] Shapiro N M, Campillo M. 2004. Emergence of broadband Rayleigh waves from correlations of the ambient seismic noise. Geophys. Res. Lett. 31 (7): L07614, doi: 10.1029/2004GL019419.

[20] Sabra K G, Gerstoft P, Roux P et al. 2005. Extracting time-domain Greens function estimates from ambient seismic noise.

[21] Bensen G. D, Ritzwoller M. H, et al. 2007. Processing seismic ambient noise data to obtain reliable broad- band surface wave dispersion measurements. Geophys. J. Int. 169, 1239-1260.

[22] Yao H J, van der Hilst, R. D., de Hoop M V. 2006. Surface-wave array tomography in SE Tibet from ambient seismic noise and two-station analysis-I. Phase velocity maps. Geophys. J. Int. 166 (2): 732-744.

[23] Shapiro N M, Campillo M, Stehly L, et al. 2005. High-resolution surface-wave tomography from ambient seismic noise. Science, 307 (5717): 1615-1618.

[24] Lin F C, Morgan P M, Michael H R. 2007. Surface wave tomography of the western United States from ambient seismic noise: Rayleigh and Love wave phase velocity maps. Geophys. J. Int. doi: 10.1111/ j.1365-246X.2008.03720.

[25] Ritzwoller M H., Levshin A L. 1998. Surface wave tomography of Eurasia: group velocites. J. Geophys. Res., 1 03, 4839-4878.

[26] Tarantola A, Nercessian A. 1984. Three-dimensional inversion with blocks. Geophys. J. R. Astr. Soc., 76 (2): 299-306.

[27] Yao H J., Beghein C., ven der Hilst, R D. 2008. Surface wave array tomography in SE Tibet from ambient seismic noise and two-station analysis-II, crustal and upper-mantle structure. Geophys J Int., 173 (1): 205-219.

[28] Yao H J, Pierre Gouedard, et al. 2011. Structure of young East Pacific Rise lithosphere from ambient noise correlation analysis of fundamental - and higher-mode Scholte-Rayleigh wave. C. R Geoscience.

[29] Herrmann R B, Ammon C J. 2004. Surface waves, receiver functions and crustal structure. Computer Programes in Seismology, Version 3.30, Saint Louis University. http://www.eas.slu.edu/People/RBHerrmann/CPS330.html.

[30] Zhang G C, Wu Q J, Pan J T, et al. 2013. Study of crustal structure and Poisson ratio of NE China by H-K stack and CCP stack methods. Chinese J. Geophys. (in Chinese). 56 (12): 4048-4094, doi: 10.6038/cjg20131213.

[31] Zhang Y Y, Gao Y, Shi Y T, Liu K. 2015. Crustal thickness and Poisson's ratio beneath Zhangjiakou-Bohai seismic active belt and its neighboring regions. Acta Seismologica Sinica (in Chinese). 37 (4): 541-553. Doi: 10.11939 /jass. 04.002.

[32] Lu Z X, Liu G, Wei M, et al. 1990. Lateral inhomogeneity of crust and upper mantle in south liaoning, China and its relationship with the M7.3 haicheng earthquake. Acta Seismologica Sinica. 12 (4): 367-378.